X-56A Flight-test Approach for Envelope Expansion Past Open-loop Flutter Instability

Christopher J. Miller, Jacob Schaefer, Matthew Boucher, Jeffrey Ouellette, and Scott Howe
NASA Armstrong Flight Research Center
Edwards, California, 93523
UNITED STATES OF AMERICA

Chris.J.Miller@nasa.gov

ABSTRACT

Contemporary aircraft are designed such that flutter instabilities lie well outside of the operational envelope. The structural stiffness required for passive flutter stability with acceptable margins is a major driver of the weight of the structure of an aircraft. The X-56A Multi-Utility Technology Testbed (Lockheed Martin, Bethesda, Maryland, U.S.A.) unmanned aircraft were built to explore the coupling of structural modes, aerodynamics, and rigid-body dynamics; and to test active means of controlling the fully coupled dynamics, including the suppression of unstable flutter mechanisms. The goal is to develop modeling and control technologies that enable highly optimized aircraft designs that do not require extra structural weight to maintain passive flutter stability margins. Flight-testing an aircraft with unstable flutter mechanisms inside the operational envelope presented significant challenges. This paper presents the flight-test approach developed for the X-56A aircraft, including the use of modeling and simulation, control and flutter margin design and test requirements, flight-test maneuvers and data analysis approach, and ground control and pilot station layout and utilization. Also discussed are some unexpected challenges that arose from the increased flexibility of the aircraft, which resulted in several takeoff and landing incidents. The flight-test program was highly successful, with 31 flights in the flexible-wing configuration. The X 56A aircraft were successfully operated at almost 10 percent beyond the open-loop flutter airspeed, and a significant amount of flight-test data was collected beyond the open-loop flutter instability. The project developed, refined, and validated many flight-test techniques applicable across a wide array of aircraft development programs. The successes and failures of this project present significant lessons learned for the development and flight-testing of future similar aircraft.

1.0 PROGRAM BACKGROUND

The X-56A Multi-Utility Technology Testbed (Lockheed Martin, Bethesda, Maryland, U.S.A.) was built by Lockheed Martin under contract from the Air Force Research Laboratory (AFRL) for the purpose of researching means of active suppression of flutter instabilities and collecting flight data for advancing state-of-the-art modeling techniques of fully coupled dynamics (Ref. 1 Beranek; Ref. 2 Ryan). Testing aircraft with flutter instabilities within their operational flight envelope is inherently high-risk for the aircraft, in part due to a lack of validation data for modeling and control techniques for flutter suppression. The X-56A aircraft were remotely piloted and designed to be relatively inexpensive to enable executing such an inherently high-risk flight-test program. The aircraft, however, were also designed and constructed in such a way that they were realistic testbeds for the relevant physics applicable to full scale aircraft.

This paper discusses the National Aeronautics and Space Administration (NASA) flight-test approach for the X-56A aircraft in the flexible-wing configuration and the key enablers to successfully accomplishing the research objectives. As well, lessons learned are identified that may be applicable to the flight-test and operation

of aircraft with similar challenges.

2.0 SYSTEM DESCRIPTIONS

The X-56A research system consisted of two reconfigurable aircraft and a versatile ground control station (GCS). The aircraft were designed such that a centerbody which housed all of the critical aircraft systems could be fitted with different wing sets based on the objectives of a given flight-test phase. In all, two centerbodies, one set of stiff wings (flutter outside of the operational envelope), and three sets of flexible wings (flutter inside the operational envelope) were manufactured. The GCS contained the pilot and co-pilot stations, real-time monitoring stations for each engineering discipline, and a pilot-in-the-loop simulation of the aircraft used for training, mission rehearsals, and qualitative evaluations of modeling updates.

2.1 Aircraft

The X-56A aircraft was a tailless, swept-wing configuration. Figure 2.1-1 is a photograph of the aircraft in flight in the flexible-wing configuration. Figure 2.1-2 is a photograph of the X-56A aircraft during preflight and shows the scale of the aircraft. Figure 2.1-3 shows the control surface and sensor layout, including wing flaps (WF) 1 through 4 on the left (L) side and the right (R) side; and the L and the R body flaps (BF). The aircraft had a 28-ft wingspan; a maximum takeoff weight of 550 lb; 10 trailing-edge control surfaces; fixed vertical winglets; and a fixed tricycle-configuration landing gear. The centerbody was constructed from carbon fiber composites with honeycomb bulkheads. The wings were a conventional structural design with fore and aft wing spars, and wing ribs constructed from carbon fiber composites. The stiff wings had carbon fiber skins and flutter modes outside of the operational envelope, and the flexible wings had fiberglass skins and flutter modes inside the operational envelope. The focus of this paper is the aircraft with the flexible wings installed. The aircraft was outfitted with a ballistic recovery parachute system which could be triggered as part of the flight termination system (FTS). The recovery system was intended to save the centerbody in the event of a catastrophic wing failure during flutter testing. The powerplant consisted of two JetCat P-400 engines (JetCat, Ballrechten-Dottingen, Germany). The aircraft had a substantial suite of instrumentation, including:

- three single-axis high-rate MEMS gyros in the nose;
- an Inertial Navigation Unit and a global positioning system (GPS) near the center of gravity;
- 10 vertical z-axis accelerometers in the wings, nose, and tail;
- a horizontal x-axis accelerometer in the nose;
- lateral y-axis accelerometers in the vertical winglets;
- a pitot-static nose boom with angle-of-attack and sideslip vanes;
- strain gauges for measuring the wing-root bending moment; and
- a Fiber Optic Strain Sensing system (installed for NASA flexible-wing flights only).

Figure 2.1-1: The X-56A Multi-Utility Technology Testbed (Lockheed Martin, Bethesda, Maryland, U.S.A.) in flight.

Figure 2.1-2: The X-56A Multi-Utility Technology Testbed (Lockheed Martin, Bethesda, Maryland, U.S.A.) during preflight.

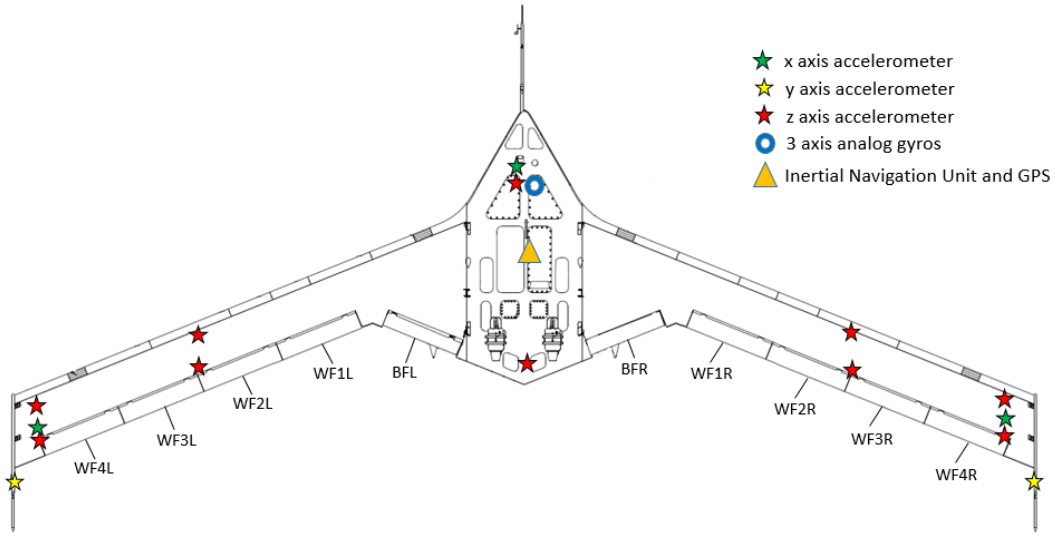

Figure 2.1-3: The layout of the X-56A aircraft sensors and control surfaces.

2.2 Ground Control Station and Simulation

The GCS served three important functions for the X-56 project: cockpit with pilot and co-pilot stations, mission control room with discipline engineers monitoring real-time data, and non-linear pilot-in-the-loop simulation for full mission rehearsals and qualitatively evaluating model updates. Integrating all of these functions and co-locating the flight crew and discipline engineers in a single facility was a key capability that enabled greater test efficiency, improved communication and situational awareness, and exceptional crew resource management. Due the time criticality of flutter-related calls, the short duration of the X-56A missions, and the limited size of the high-risk unmanned aircraft systems test range, having a high degree of team cohesion and crisp communication was of paramount importance. Figure 2.2-1 is a photograph of the GCS during preflight for an active mission.

Figure 2.2-1: The X-56A ground control station.

The most critical function of the GCS is that of the cockpit (Figure 2.2-2). One significant challenge of all remotely operated aircraft is the fact that pilot and copilot situational awareness (for example, the absence of engine noise and motion cues) is reduced by not being physically onboard the aircraft. The pilot stations and displays interface to the aircraft by way of a bi-directional command and control (C2) serial link. The pilots send commands to the aircraft by way of inceptors (side stick, rudder pedals, and dual throttles) and mission system interfaces. The aircraft uses this same link to send back state and warning message information, which is then displayed on the pilot station displays. The out-the-nose video used by the pilots to fly the aircraft based on visual references is transmitted to the ground by way of a video transmitter and is displayed to the pilots with a head-up-display (HUD) overlay of the aircraft state data. Artificial out-the-nose graphics are generated using the C2 aircraft state data as a backup visual reference in the event of the loss of downlinked nose video and for flight simulation and mission rehearsals. Figure 2.2-2 is a photograph of the pilot station and the and co-pilot station. The top two large displays provide live video feed from a configurable external camera view of the aircraft (typically a view from the ground beside the runway) and a moving map display that is independent of the aircraft C2 data link. The smaller wall-mounted monitors display out-the-nose video with the HUD overlay. Figure 2.2-3 shows a close-up of the two lower head-down displays (HDDs) at the left seat. The display on the left has a large configurable moving map display with flight path predictors, runways, and airspace boundaries. The buttons above the moving map display allow the pilot to configure the aircraft systems, including braking forces, engaging backup control modes accounting for failures such as loss of GPS or air data, configuring and arming takeoff and landing modes, and engaging and disengaging research control laws. In the lower right-hand corner of that display is a menu enabling the pilot or copilot to configure and engage research test maneuvers by way of the flight-test aids (FTAs). The right-hand display in Figure 2.2-3 displays more detailed aircraft state information than is displayed in the HUD. Engine parameters including revolutions per minute (RPM) and exhaust gas temperature (EGT), and fuel pump voltage, fuel level, and main battery voltage are displayed along the right-hand side of that lower display. In the bottom right-hand corner of the display is a set of indications for warnings and cautions, and along the bottom in the middle is a display showing control surface positions, nosewheel steering position, and braking indications including the parking brake. For warnings and cautions, in addition to the display in the lower right, an audible “warning” or “caution” is annunciated in the pilot and copilot headsets, and hash marks are displayed in the middle of the HUD, cueing the pilot to look down at the HDD to identify which warning or caution has been triggered. In the upper left-hand corner of the display is an indication of C2 message integrity, active C2 antenna (upper or lower), and buttons indicating the control mode (auto/lost link, or manual/piloted).

Figure 2.2-2: The pilot station (left); and the co-pilot station (right).

Figure 2.2-3: Close-up of pilot station head-down displays.

The GCS also functions as the mission control room during flight operations where discipline engineers monitor real-time data. A small group of engineers are collocated with the pilots and the mission controller during flights (Figure 2.2-1). This group monitors the real-time telemetry data from the aircraft for the purposes of monitoring flight safety and mission success. The GCS had the ability to drive up to nine real-time data displays from five independent computer consoles. The GCS also had stations for a Mission Controller and a Project Manager (PM). The disciplines in the control room for the X-56A missions were flight controls, structures, and flight systems. Figure 2.2-4 shows the layout of the GCS as a control room including the console and communication (Com.) panel locations. The minimum GCS crew for a research mission consisted of:

- a pilot and copilot responsible for operating the aircraft,
- a mission controller responsible for coordinating communication and conducting the mission,
- two flight controls discipline engineers for monitoring the aircraft dynamics and control law parameters,
- one or more Principal Investigators with detailed knowledge of the control system under test,
- two structures engineers monitoring the structural loads and dynamics of the aircraft,
- one systems engineer monitoring aircraft system parameters such as voltages and temperatures,
- a PM responsible for overall mission execution, and
- a test information engineer (TIE) who ensured operation of critical control room functions such as real-time data displays.

Outside of the GCS is the Range Safety Officer, who manages the FTS and ensures the aircraft remains in the allocated airspace, and a Range Control Officer, who ensures that external range systems such as radios, telemetry, and communication equipment are functional.

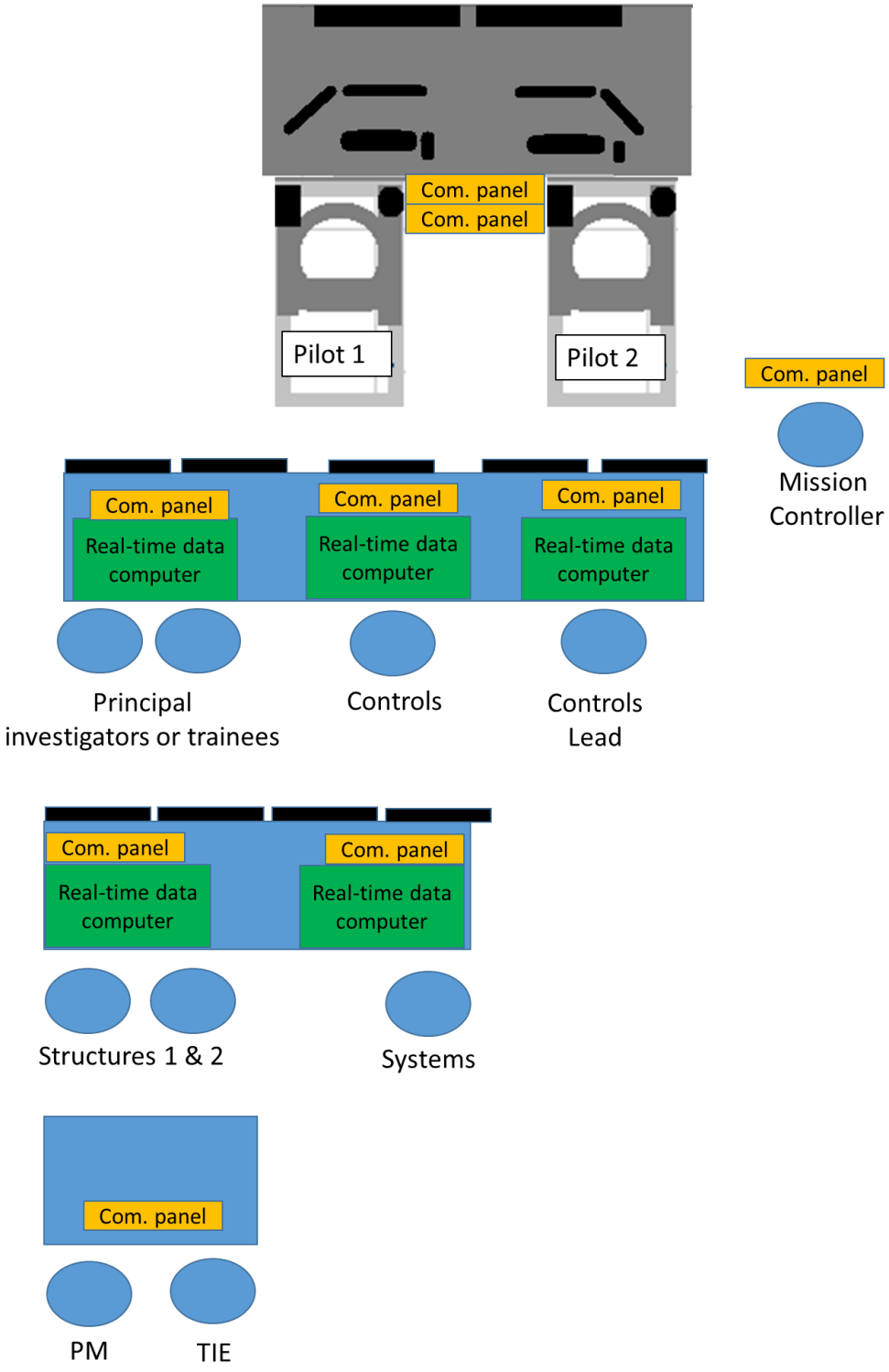

Figure 2.2-4: The layout of the X-56A ground control station.

The GCS also was a fully integrated simulation facility. The simulation interfaced with the same cockpit hardware, software, and displays used for the flight configuration, with the capability to drive real-time data displays for the discipline engineer stations. This fully integrated facility allowed the X-56A project team to perform realistic mission rehearsals, which were critical due to the very compressed, fast pace of the X-56A flight missions as well as the time- and safety-critical calls necessary for flutter testing.

3.0 FLIGHT-TEST APPROACH

The NASA flight-testing of the X-56A was conducted in two phases. The first flights were performed with the stiff wings installed to check out the aircraft and GCS systems, and to gather flight data to validate modeling techniques that would be critical for developing models and control laws for the later flexible-wing flights. The NASA conducted eight flights with the stiff wings installed and successfully completed all of the primary objectives with the stiff wings. Upon the landing of the eighth NASA flight, however, the aircraft (centerbody and stiff wing set) was damaged due to a divergent mode that was triggered by a nose landing gear problem (Ref. 3 Baumann). Shortly after the NASA landing incident, Lockheed Martin attempted their first flight with the flexible wings installed and encountered a problem during takeoff that destroyed the other centerbody and one set of flexible wings (Ref. 4 Howe). The initial aircraft design and flight-test planning efforts were conducted under the assumption that the highest-risk portion of the flight-testing would be at or near the flutter instability. These two incidents, however, uncovered some significant challenges related to takeoff and landing for flexible flying-wing aircraft and triggered significant analysis and redesign efforts prior to the NASA flexible-wing flights.

3.1 Takeoff and Landing Challenges

The configuration of the X-56A aircraft presented some unique takeoff and landing challenges. First, the aircraft was designed to be configurable with a range of center of gravity locations including static instability. The main landing gear thus needed to be farther aft of the aerodynamic center than would have otherwise been desirable. The aft main gear location, combined with the lack of a horizontal tail, resulted in an aircraft that was very difficult to rotate on takeoff. Additionally, the wing flexibility creates a situation in which upon rotation the wings bend up rapidly due to the quick onset of lift, resulting in a pitch-up moment due to the aft wing sweep. These factors combine to create a situation on takeoff that can cause a rapid uncontrollable pitch-up and results in either an over-g or stall condition. Thus NASA reconfigured the aircraft prior to their flexible-wing flights to have a slightly nose-high attitude on the ground to reduce the amount of rotation required on takeoff, and to reduce the lift transient. These modifications, however, created a situation in which rejected takeoffs were not feasible due to the high-slung engines. A reduction in thrust on takeoff would result in a net pitch-up moment that could have caused the aircraft to rotate and lift off below stall speed. Configurable landing gear that would have allowed control of the pitch attitude of the X-56A aircraft during the takeoff roll would have been a much better solution, however, the mechanical complexity and additional weight did not make sense for the X-56A application.

The lack of a horizontal tail and the location of the aft main gear resulted in very little control of the nose de-rotation on landing. This problem was compounded by the fact the landing gear was designed to survive a parachute landing, meaning the gear was stiffer than would have otherwise been desired. These two factors meant that very high loads were imparted to the nose gear on landing, and that a significant amount of energy went into the structure of the aircraft, including the flexible wings, rather than being absorbed by the landing gear. During the eighth NASA stiff-wing flight, the nose gear strut bound due to these high loads, and a nearly elastic nose bounce resulted. The aircraft eventually pitched up and stalled a few feet above the runway and

made a hard landing. Thus, NASA redesigned the nose landing gear system to absorb more energy and to reduce the probability of binding prior to their flexible-wing flights; however, during ground tests prior to flight, it was discovered that the additional wing flexibility exacerbated the tendency of the nose to bounce due to coupling between the wings and the landing gear. That situation, combined with the higher nose attitude on the ground used to address the takeoff challenges, meant that passive means alone were insufficient to mitigate nose bounce landing problems. An active landing mode control system that did not require any new sensor or controls surfaces was implemented that utilized nose vertical acceleration to damp out any sensed nose bouncing. This controller proved to be very effective at damping out these undesired dynamics.

It is worth noting that none of these challenges were predicted prior to flight. Much attention was paid to the risks posed by flight past the open-loop flutter instability, but the project team was late to recognize the effects that the wing flexibility would have even at the relatively low speeds of takeoff and landing. In the end, specialized control laws were needed for both takeoff and landing. These control laws were classical in nature and were used throughout the flexible-wing flight phase. The flutter suppression control laws were only activated up and away, and were never used for takeoff and landing.

3.2 Flutter Envelope Expansion with the Flexible Wings

Flight-testing at speeds above the open-loop flutter instability is something that not many research programs have accomplished, at least not intentionally. Flight above the flutter speed is inherently risky due to the explosive nature of flutter instabilities. The uncertainty related to the modeling fidelity in that region added to the risk of the X-56A project because there were no data available to validate the accuracy of the models. The flutter mechanism for the X-56A aircraft complicated the modeling task as well because it involved coupling between rigid-body and structural modes (Ref. 1 Beranek, Ref. 5 Ouellette). Most flutter mechanisms only involve structural modes. The X-56A flight-test approach utilized specialized FTAs and a cautious build-up approach utilizing real-time monitoring, control law margin and performance metrics, and post-flight data analysis to successfully expand the envelope up to and beyond the open-loop flutter instability.

3.2.1 Flight-test Maneuvers

The X-56A flight systems enabled the design and activation of automatic flight-test inputs that could be injected at any point in the control loops or sent directly to the control surfaces of the aircraft. These FTAs were used extensively for generating data used for determining control law performance, controller-loop margins, modal frequency and damping, and for extracting basic aircraft modeling data by way of parameter estimation (Ref. 6 Grauer, Ref. 7 Grauer). The FTAs were entered by the co-pilot and activated once the pilot established a stable flight condition and the mission controller verified the FTAs were entered correctly. The pilot is able to actively control the aircraft while the FTA is executing. A normal integrated test block used to clear a new flight condition followed the sequence:

- frequency-tuned surface rap FTAs to enable the assessment of modal damping and system stability (Figure 3.2.1-1);
- pilot pitch and roll captures to assess piloted flying qualities;
- multisine control input FTAs used for post-flight control-loop margin assessments; and
- multisine control surface FTAs used for post-flight parameter estimation and model tuning (Figure 3.1.2-2).

The frequency-tuned raps were designed to excite modes between 10 and 25 rad/s. This frequency range

captures first wing bending at subcritical airspeeds and the flutter mechanism at supercritical airspeeds (Figure 3.2.1-1). The raps could be performed with the control loops open or closed. The closed-loop raps were used for assessing closed-loop damping as a measure of controller performance. The open-loop raps were utilized for assessing the open-loop plant modal damping and stability properties.

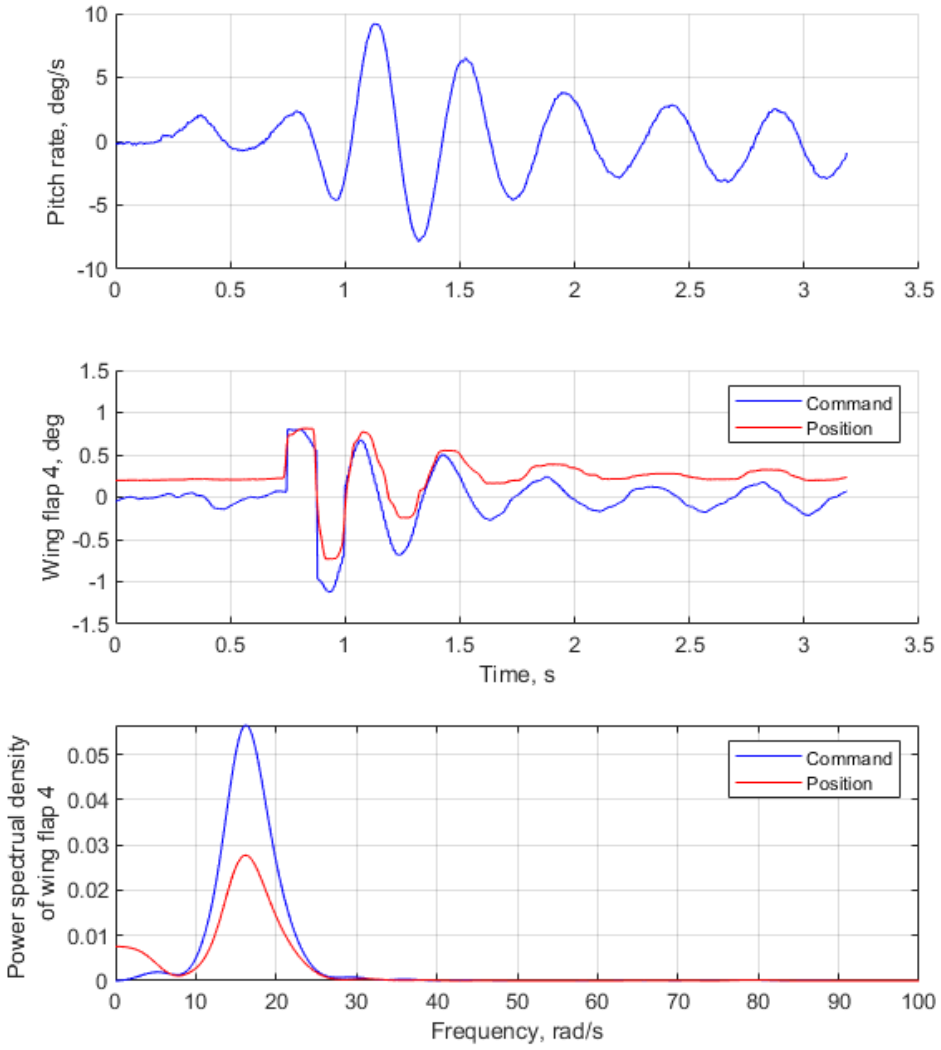

Figure 3.2.1-1: Example of a rap maneuver.

Figure 3.2.1-2 and Figure 3.2.1-3 show an example of a multisine maneuver that excites all 10 control surfaces simultaneously. Figure 3.2.1-2 shows how the input power is distributed between the different control surfaces and shows the power at each discrete input frequency. Figure 3.2.1-3 shows how the test inputs are resolved in the time domain.

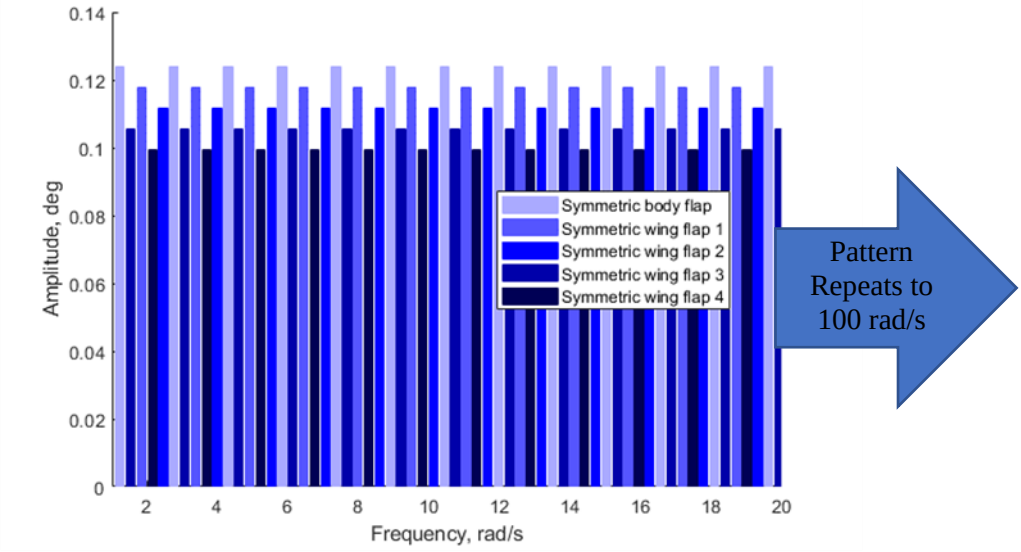

Figure 3.2.1-2: Example of a multisine maneuver: Distribution of power between different control surfaces.

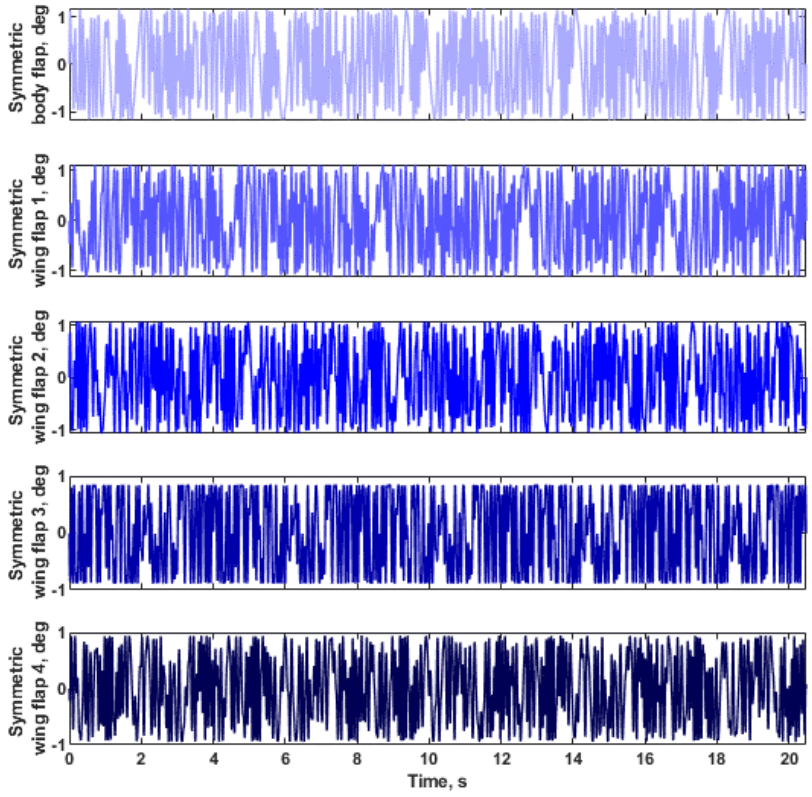

Figure 3.2.1-3: Example of a multisine maneuver: Test inputs resolved in the time domain.

As airspeeds increased, more than one flight was required in order to obtain all of the necessary data to clear a given flight condition because the fundamental flutter dynamics change as the center of gravity shifts forward as fuel burns off due to the strong coupling between the rigid-body (short-period) and the structural modes (first wing bending). The ability to design and execute these highly specialized multisine inputs was a critical part of the flight testing, reducing the amount of time required for each maneuver by approximately a factor of three when compared to traditional logarithmic frequency sweeps. Flight-testing at higher speeds may not have been feasible with traditional logarithmic frequency sweep maneuvers due to the long durations required to sweep through the desired frequency range. Those long-duration maneuvers would have been problematic due to the limited airspace available for testing, and the fact that the dynamics of the aircraft change as fuel burns off (the characteristics of the aircraft are different at the beginning of the maneuver and the end of the maneuver).

3.2.2 Real-time Monitoring

The ability to monitor real-time flight data in the GCS was critical for envelope expansion and for ensuring good quality data for post-flight analysis. To facilitate envelope expansion both flight controls and structures engineers monitored accelerometer data to determine if there were any stability or performance issues. The engineers primarily observed the closed-loop frequency and damping dynamics generated by the rap maneuvers. Because the team was able to practice missions prior to flight, they were able to watch for any apparent differences inflight. Additionally, they watched for actuator rate limiting and saturation, which would have effectively opened the loop and resulted in loss of control of the unstable mode. They also watched for limit-cycle oscillations (LCOs) as an indicator of instability. The actuators had a small dead-zone wherein they did not respond to small commands, which was effectively an open-loop region. The magnitude of the resulting LCO was a good indication of the level of instability.

3.2.3 Control Law Envelope Expansion

The flutter suppression controls necessitated more than the traditional single-loop margin assessments to determine robustness prior to flight. The controllers were assessed against a range of requirements to determine if they were adequately robust, including single-input single-output gain and phase margin, Mu uncertainty margins, and Monte Carlo based uncertainty assessments.

During envelope expansion the controller needed to demonstrate robust performance prior to testing at the next higher flight speed. The controller needed to meet predefined closed-loop damping and gain and phase margin on all critical loops. When the controller no longer met these requirements in flight, envelope expansion testing was paused, and the controllers were re-tuned using the lower-order equivalent system (LOES) models and updated high-order linear models. Additionally, the LCO that resulted from the actuator dead-zone was required to be less than a predefined pitch rate and not adversely affect piloted flying qualities.

3.2.4 Flight Condition Test-point Order

Flutter instability for the X-56A aircraft occurred at the lowest airspeed with forward center of gravity (low fuel). The flutter mechanism that caused the instability was a coupling of the short-period and first wing bending of the aircraft. Thus the mass and center of gravity of the aircraft play a substantial role in the flutter mode characteristics. Expansion was performed at a constant airspeed and with decreasing fuel mass. The airspeed was nominally increased 10 kn at airspeeds with more than 10 percent predicted open-loop flutter margin and every 5 kn thereafter.

The unstable coupling worsens as the aircraft burns fuel, thus it was critical that the project team utilize the rap

maneuvers and a real-time assessment of the closed-loop damping to determine the risk associated with continuing. At each new airspeed the GCS crew attempted to execute a rap (to assess stability), the two FTAs required to assess loop margins post-flight, and a system identification FTA designed to assess model fidelity and update models post flight. The project team repeated this cycle as many times as possible until either lower-than-desired closed-loop damping was witnessed, or bingo fuel level was reached.

Additionally, at each new airspeed, a calibration check was performed with the chase airplane. This check was simply an airspeed cross-check, not a rigorous air data calibration (air data calibration had been performed earlier, during the stiff-wing flight tests). No problems with airspeed calibrations were apparent even well past the open-loop flutter instability.

As the open-loop flutter speed was approached, there appeared to be a low-level persistent oscillation following raps while at elevated g levels in level turns. Therefore, turns were conducted at a reduced airspeed until closed-loop damping assessments could be made for turns at higher airspeeds. The oscillations in at elevated g levels were believed to be related to changes to the overall structural stiffness due to the increased wing loading and the resulting changes in the coupled modes. Ultimately, no problems were found that resulted in controller performance concerns during turning flight, but it was important to have explored this type of flight, given the unknowns related to active control of these coupled dynamics.

3.2.5 Envelope Expansion Data Analysis

A significant amount of post-flight data analysis was performed between envelope expansion flights to determine if it was safe to expand the envelope further. The following needed to be evaluated between flights: modal frequency and damping assessments, controller loop margins, and system identification for model validation.

Two types of multisine inputs were used for frequency response reconstructions and parameter estimation. The first type was designed to excite single control loops or simple combinations of loops primarily for the purpose of generating post-flight frequency responses used for evaluation of control margins. The second type was designed to excite the dynamics of the aircraft with a single maneuver with sufficiently rich linearly independent inputs for the purposes of system identification. Figure 3.2.1-2 shows a system identification example wherein all 10 control surfaces are excited simultaneously in symmetric pairs used for system identification in the longitudinal axis. Both types of multisines were designed to be periodic such that they would repeat the same input after a specified time frame. This repetition permitted windowing and averaging across different cycles of a single maneuver. Both types also generate input power at discrete frequencies, which permits the analyses to be performed at the known frequencies, which reduces the influence of measurement noise and turbulence. The single-loop type by design produced the cleanest frequency responses with the highest coherence for the loop excited, and system identification type resulted in the best data for identifying broad aspects of the dynamics of the aircraft from a single maneuver including multi-input-multi-output frequency responses (Ref. 5 Grauer). The single-maneuver-derived reconstructed frequency responses were not used for margin determination; however, they were critical for picking out key features such as modal frequencies and damping, at supercritical airspeeds due to the rate of change of the plant due to fuel burn.

Another important analysis that was used for assessing multiple envelope expansion metrics was the derivation of LOES (Ref. 8 Morelli, Ref. 9 Mitchell) models from the flight-test data generated by the multisines. These LOES models were generated at each new airspeed and fuel mass combination. The LOES transfer functions as presented in this paper were derived in two different ways. The first method used a time-domain-output-error-based recursive non-linear least-squares approach. The second method utilized the reconstructed frequency

responses from the single-maneuver all-surface approach mentioned above. Both methods simultaneously fit the multi-input multi-output system to a set of sixth-order transfer functions. The poles for all of the system transfer functions were the same and were assumed to take the form of three complex poles that represented the short-period mode, symmetric wing first bending, and symmetric wing first torsion. At subcritical speeds, both techniques produced similar results for modal frequencies and damping numbers. The time domain approach, however, showed the least sensitivity to noise and the type of maneuver used, as well as producing the best estimates of the numerator coefficients because by performing the fits in the time domain all inputs and outputs are coupled during the fitting process. The frequency domain technique requires the additional step of performing the frequency reconstruction prior to doing the LOES fit. This step introduces additional uncertainty; the numerator coefficients for each transfer function are independent during the LOES fit. One significant limitation of the time-domain LOES fitting technique is that when identifying an unstable open-loop plant the controller must be included in the identification. The known controller must be used to stabilize the open-loop unstable plant during the time-domain identification process, otherwise the instability causes the simulated data sets used for driving the recursive least-squares to be divergent. This result proved to be a problem for the X-56A system at supercritical airspeeds due to non-linearities in the actuators producing apparent deadzones (Ref. 10 Pankonien). Because the frequency-domain technique does not require simulation of the identified plant, measured surface positions can be used instead of controller commands, making this technique less sensitive to actuator non-linearities when fitting the bare airframe. Overall, the time-domain approach was used for subcritical airspeeds because it showed the least variability and produced results that could be used for control system design because of superior fitting of the numerator coefficients. The frequency-domain approach was used at supercritical airspeeds due to the actuator non-linearities. In Reference 10 Morelli presents other techniques for determining LOES fits and discusses some of the practical implications of the different techniques.

The LOES models were used to determine the open-loop modal frequency, and damping for the pertinent modes, and to predict the condition at which the coupled modes would be open-loop unstable (flutter). Additionally, up to the point of instability these models were used to make design changes and evaluate new control laws prior to flight. In other words, when flight-determined control law margins dipped below the required margins, the LOES models were used to determine and evaluate the design changes necessary to restore acceptable margins and continue envelope expansion. Figure 3.2.5-1 and Figure 3.2.5-2 show an example of the time-domain comparison between the LOES model and the actual flight data at 90 kn and 50 lb of fuel. Figure 3.2.5-1 shows the the LOES captures the large scale dyamics for the full duration of the manevuer, and Figure 3.2.5-2 shows that the the LOES accuratly caputes the smaller scale dynamics. All seven sensors were fit simultaneously and include the contributions from all 10 (5 symmetric pairs) of control surfaces. The fits can be seen to be fairly good for all of the sensors as there are no significant features apparent in the time domain that are not captured by the LOES fits.

Clockwise from lowest left, Figure 3.2.5-1 and Figure 3.2.5-2 show data for the centerbody aft z accelerometer (CAZ); the centerbody forward z accelerometer (CFZ); pitch rate (q); the symmetric outboard forward z-axis accelerometers (Sym. OFZ); the symmetric outboard aft z-axis accelerometers (Sym. OAZ); the symmetric midspan forward z accelerometers (Sym. MFZ); and the symmetric midspan aft z accelerometers (Sym. MAZ).

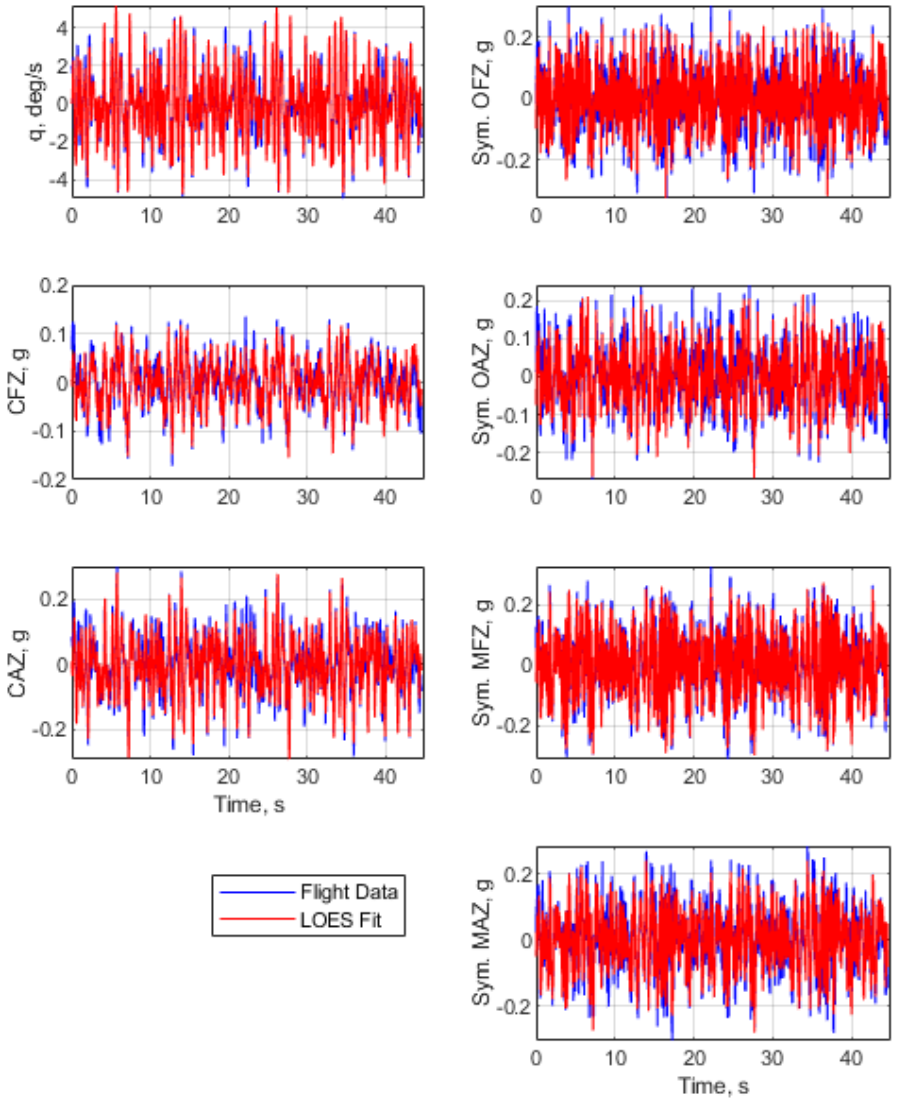

Figure 3.2.5-1: Example of a time-domain fit for low-order equivalent system for 90 kn and 50 lb of fuel.

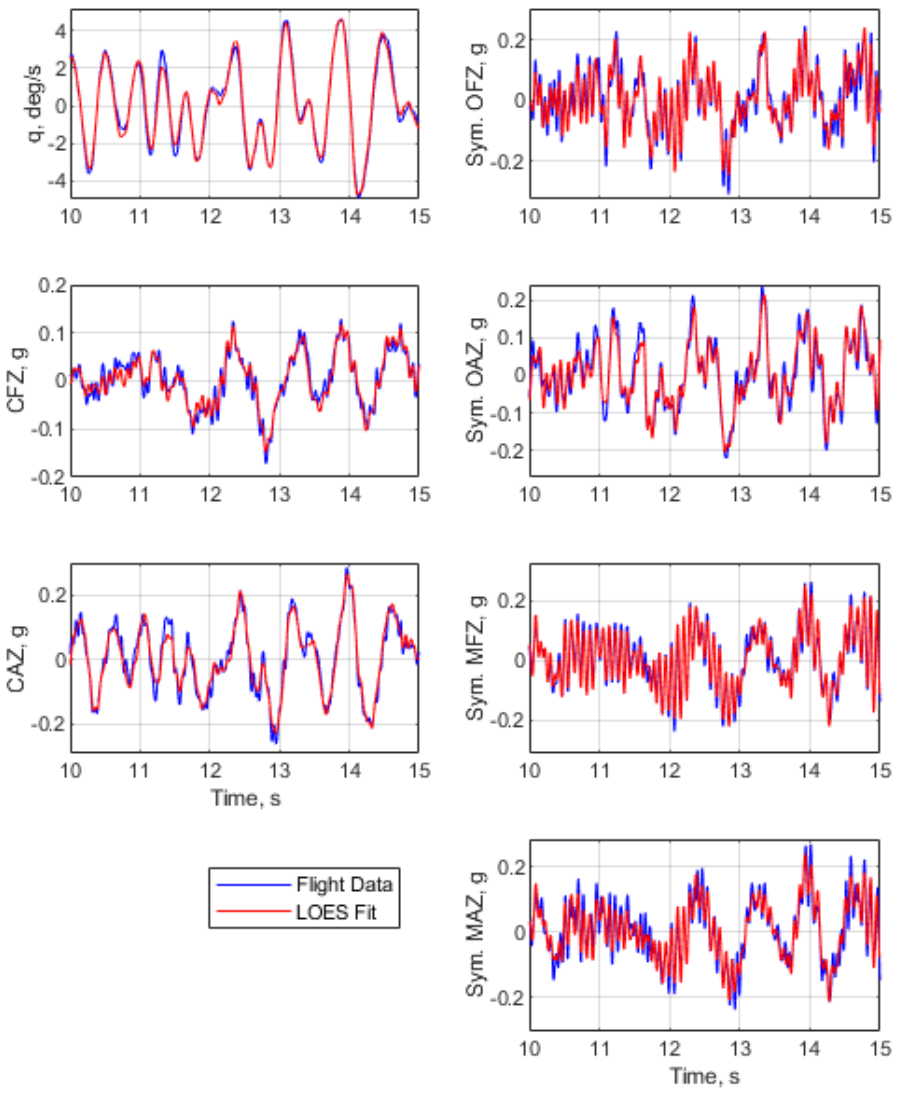

Figure 3.2.5-2: Zoomed view of a time-domain fit for 90 kn and 50 lb of fuel.

Figure 3.2.5-3 shows an example of a high-quality frequency response reconstruction of the elevator loop at 90 kn and 50 lb of fuel, and how that frequency response compares with both the preflight model prediction (Ref. 5 Ouellette) at that condition, and the frequency response of the time-domain-derived LOES. Generally, for the frequencies below first wing bending, the three agree fairly well in both magnitude and phase; however, the flight methods both show slightly higher frequency and damping for the short-period-related peak, and a slightly higher overall magnitude at the first wing bending frequency. The three responses also have some significant differences in both phase and magnitude between the first wing bending and first wing torsion modes. The reconstructed frequency response is considered the most accurate representation of the actual frequency response of the X-56A aircraft because it is computed directly from the flight data without any assumed model formats and suggests that both the LOES and the preflight models would need to be refined if the torsional mode were critical to the flutter mechanism of concern, or if the controller was designed to affect this mode. The primary flutter mechanism of concern being a coupling of the short period and first wing bending modes, however, this

analysis suggests that the LOES and the preflight models are sufficiently accurate at 90 kn and 50 lb of fuel for both flutter prediction and control law design.

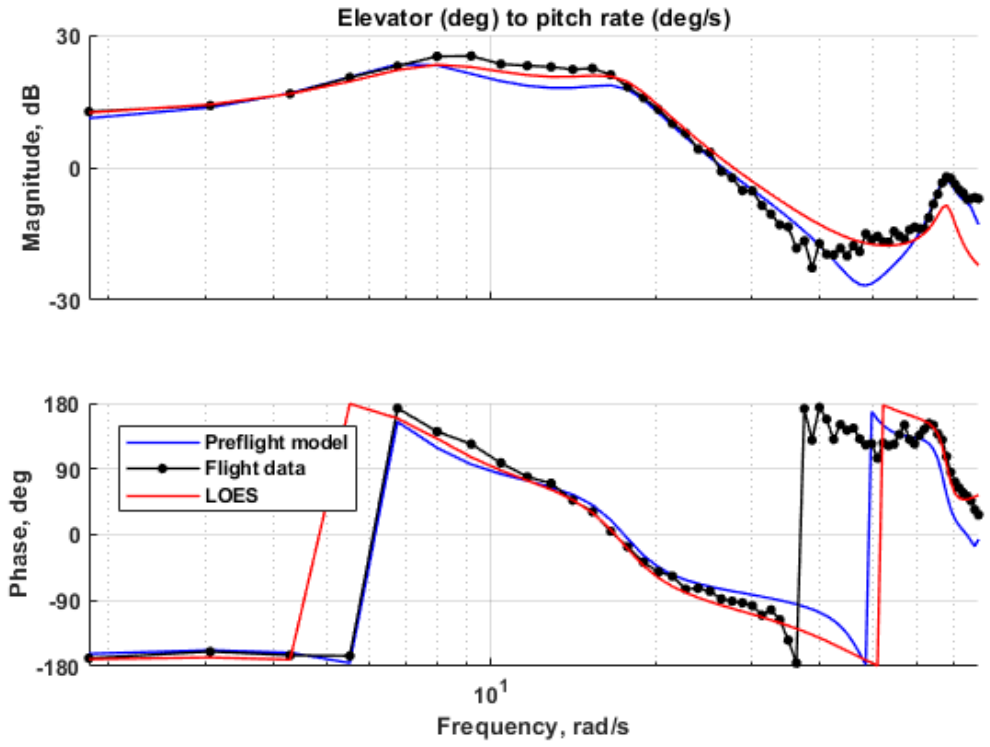

Figure 3.2.5-3: Comparison of reconstructed frequency response, low-order equivalent system frequency response, and preflight-model-predicted frequency response for 90 kn and 50 lb of fuel.

Figure 3.3.5-4 shows the results of the LOES fit to the frequency response reconstruction data for 115 kn and 20 lb of fuel. The frequency response reconstruction is noisy, which means that the results from any one transfer function fit have significant uncertainty; however, simultaneously fitting all five symmetric pairs of control surfaces (bf, wf1, wf2, wf3, wf4), and seven sensor outputs (pitch rate, outboard aft z accelerometer, outboard forward z accelerometer, centerbody forward z accelerometer., centerbody aft z accelerometer, midspan aft z accelerometer, and midspan forward z accelerometer) reduces the uncertainty on the estimates for modal frequencies and damping because the same denominator is used for each transfer function. The noisy reconstructions mean that it is very difficult to get reliable fits for the numerators of the transfer functions which are unique for every sensor and surface combination. The LOES fits using the frequency response reconstructions were too uncertain to use for control design for this reason.

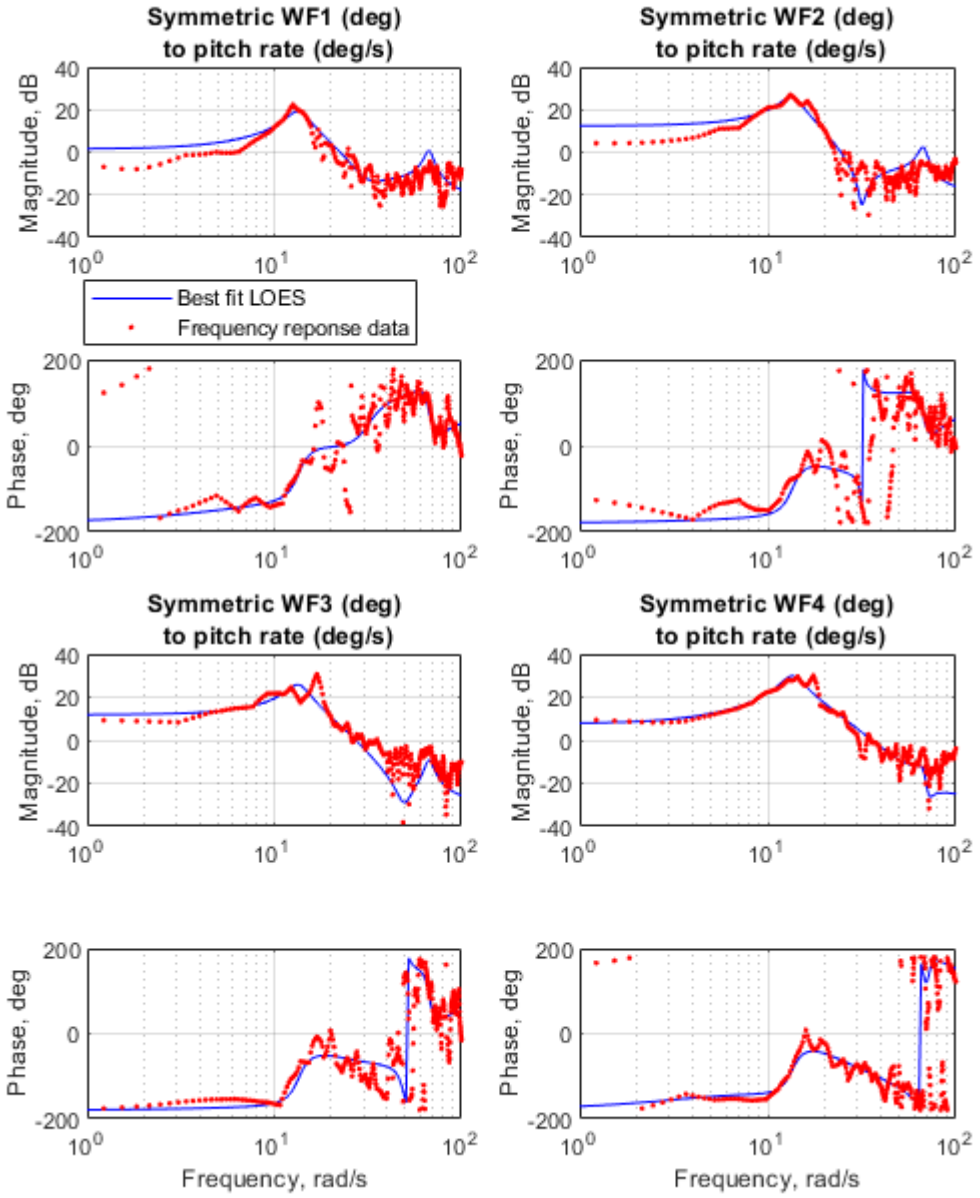

Figure 3.2.5-4: Frequency domain low-order equivalent system for 115 kn and 20 lb of fuel.

Model uncertainty, and the criticality of the control law performance and controller margins, increase as the envelope is expanded toward the open-loop flutter instability. Therefore, it was important for the project team to be able to estimate based on flight data at subcritical speeds where the flutter instability is likely to occur. The trends for modal damping for some flutter mechanisms, however, don't lend themselves well to extrapolation (Ref. 11 Zimmerman). When modes couple, such as in the case of the X-56A flutter mechanism, the modal damping for a single mode can change very rapidly with airspeed. Rather than look purely at the modal damping for a given mode and generate predictions based on extrapolation, the X-56A project team explored utilizing the Zimmerman Flutter-Margin Criterion (Ref. 9 Zimmerman). This method is based on the Routh's discriminate for

the characteristic equation of the two modes coupling that generate the flutter instability. The Zimmerman flutter margin parameter is quadratic with dynamic pressure at constant Mach number for quasi-steady aerodynamics with no structural damping. Therefore, a second order fit was used to predict where the flutter instability would occur. Figure 3.2.5-5 shows how the Zimmerman flutter prediction (Pred.) evolved as airspeed (in kn, V) envelope expansion progressed. It shows that even with just a few airspeeds the Zimmerman margin parameter did a very good job of predicting the observed flutter speeds of <110 kn for low mass and <112 kn for high mass, and was very useful at predicting how much airspeed margin remained as the project team stepped out in airspeed and down in fuel mass.

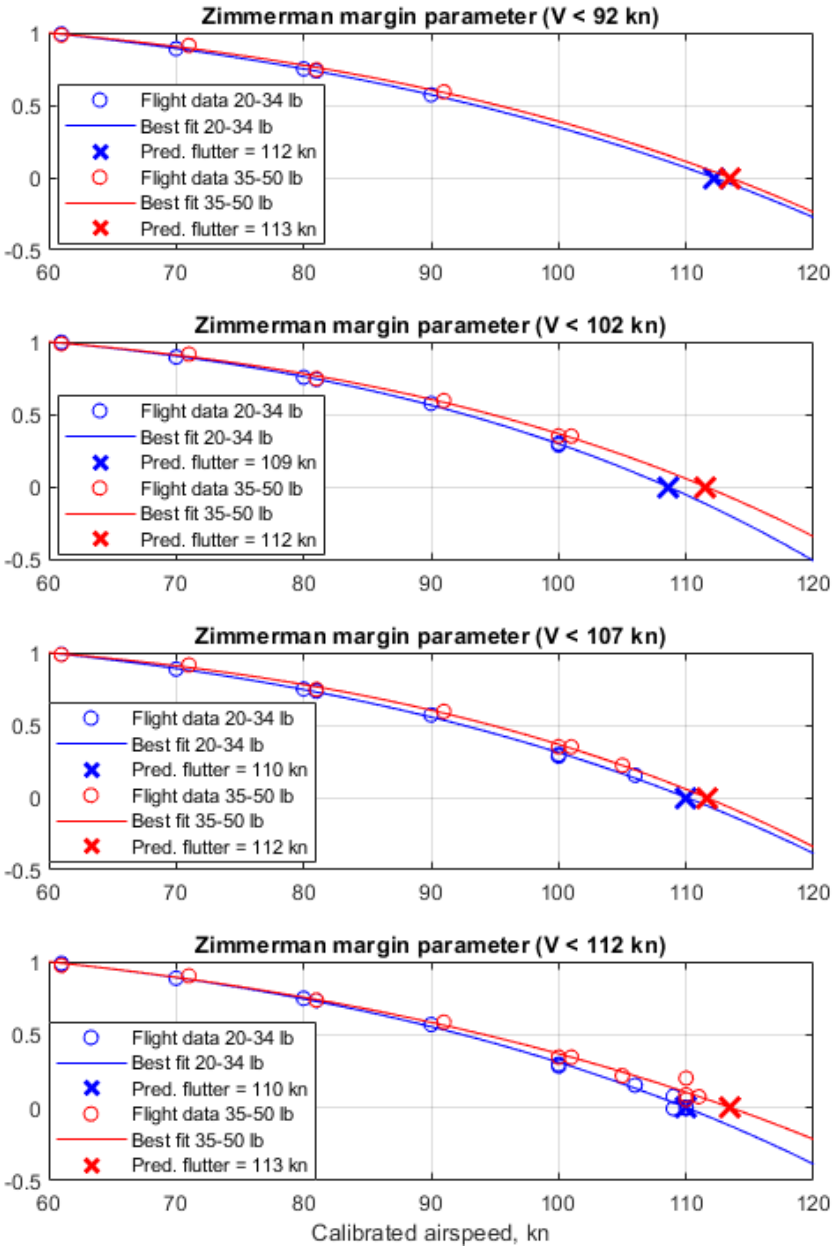

Figure 3.2.5-5: The Zimmerman flutter-margin parameter and flutter predictions with increasing airspeed.

3.3 Role of Modeling and Simulation

The tools required for predicting the airspeed for flutter instability are well established, however they were found to be insufficiently accurate for modeling the system dynamics for control system design and verification. Modeling control effects on and the coupling characteristics of the modes contributing to flutter was a significant challenge. The project team started by generating preflight linear models derived from ground-vibration-test-corrected finite element models for the structure of the aircraft, and aerodynamics models derived from unsteady potential flow-based models blended with steady aerodynamic corrections from wind-tunnel and stiff-wing flight-test data (Ref. 8 Ouellette). These models were used for control law design and analysis prior to flexible-wing flights and were continuously refined based on flexible-wing flight-test results.

These pure linear models, however, while high-order, did not lend themselves well to either piloted simulation testing or for analysis of fundamentally nonlinear flight regimes such as takeoff and landing. One of the lessons learned from the early missteps that led to the loss of one aircraft on takeoff and damage to the other on landing was that modeling the fully coupled aircraft dynamics during takeoff and landing was very important. During takeoff the flexible-wing dynamics contribute to uncertainty in the trimmed forces on the aircraft during the takeoff roll and cause a significant shift in the aerodynamic center during rotation. On landing the flexible-wing dynamics couple with the landing-gear dynamics and aerodynamic forces to produce a potentially unstable pitch mode. Techniques were developed that allowed the fully coupled dynamics to be modeled in the non-linear piloted simulation; this simulation was instrumental in developing operational procedures, special control law modes for takeoff and landing, and for pilot and GCS crew training. The linear models were the best at modeling the fully coupled flutter dynamics at the test conditions; however, without the coupled nonlinear simulation the flight-test campaign would not have been able to successfully address the fundamental takeoff and landing challenges.

Finally, as mentioned above, simple linear transfer function models were derived directly from the flight-test data. While of lower order than the preflight linear models, these models were instrumental in validating control law designs and margins, and were also very useful for identifying necessary design changes between envelope expansion test points when the more complicated linear models were not matching the flight-test data to an acceptable degree.

3.4 Other Operational Flight-test Requirements

Many things had to come together to execute this high-risk flight research project safely. Assuring that the aircraft would remain within the relatively small, restricted airspace over Rogers Dry Lake was key, and was accomplished by installing on the aircraft an FTS certified by the Range Commander's Council and utilizing an independent Range Safety Officer with the ability to terminate the aircraft. The FTS, when activated, would have terminated the aircraft by disabling the fuel pumps for range containment and deploying a ballistic recovery parachute to attempt to save the centerbody and primary flight systems. This FTS function was never utilized; however, given the high-risk nature of flight-testing beyond flutter and the low level of assurance to which the aircraft was developed, the FTS was a key part of the safety case that enabled the project team to adequately mitigate risks to ground assets and personnel.

The project team utilized piloted chase airplanes for assessing atmospheric winds and turbulence, and as an airspeed cross check. X-56A was very sensitive to atmospheric turbulence due to the highly flexible wings and the tailless configuration. Additionally, the piloted chase airplane would have served as an additional

independent set of eyes on the X-56 aircraft in the event of certain system failures. Figure 3.4-1 is a photograph showing the NASA T 34C Turbo Mentor (Beech Aircraft Company, now Raytheon Technologies, Waltham, Massachusetts, U.S.A.), a typical chase airplane in position for X-56A missions.

Figure 3.4-1: The NASA T-34C Turbo Mentor (Beech Aircraft Company, now Raytheon Technologies, Waltham, Massachusetts, U.S.A.), a typical chase airplane for the X-56A aircraft.

4.0 FLIGHT-TEST RESULTS

The flight envelope was expanded out to 120 kn, which was ~10 kn above the open-loop flutter instability at low fuel mass. Figure 4-1 shows how the frequency and damping for all three primary modes varied as a function of airspeed at both high and low fuel mass. Shown are the frequencies of the short-period and first wing bending modes converging at the flutter instability and then diverging again in the unstable region. The torsional mode is still well separated from the bending mode, suggesting significant margin prior to those modes coupling to form the next unstable flutter mechanism.

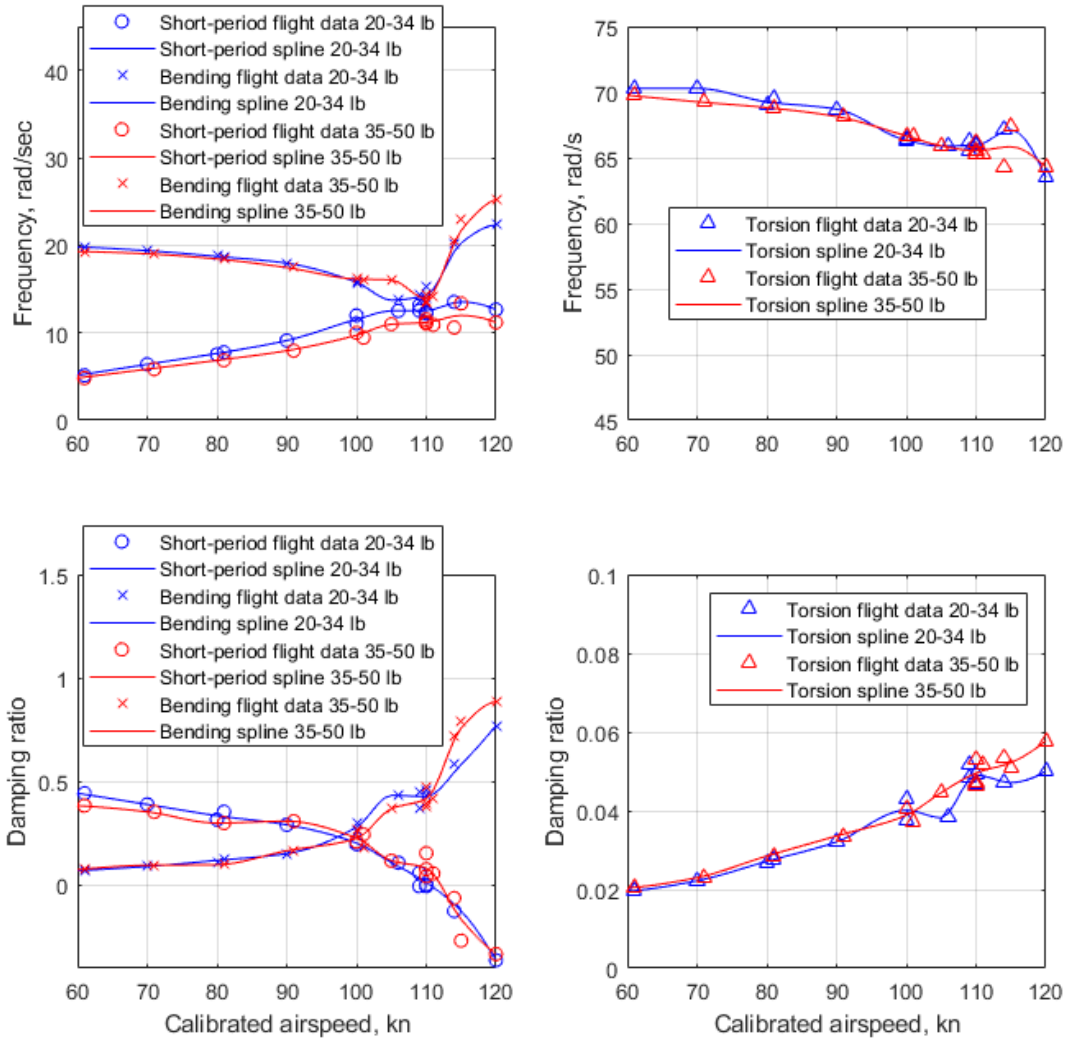

Figure 4-1: Modal frequency and damping versus airspeed.

Figure 4-2 shows how the LOES frequency response of the wing flap 4 to pitch rate transfer function varies with airspeed. The short period and bending modes converge on one another to form the flutter instability, and then they decouple again with increasing knots calibrated airspeed.

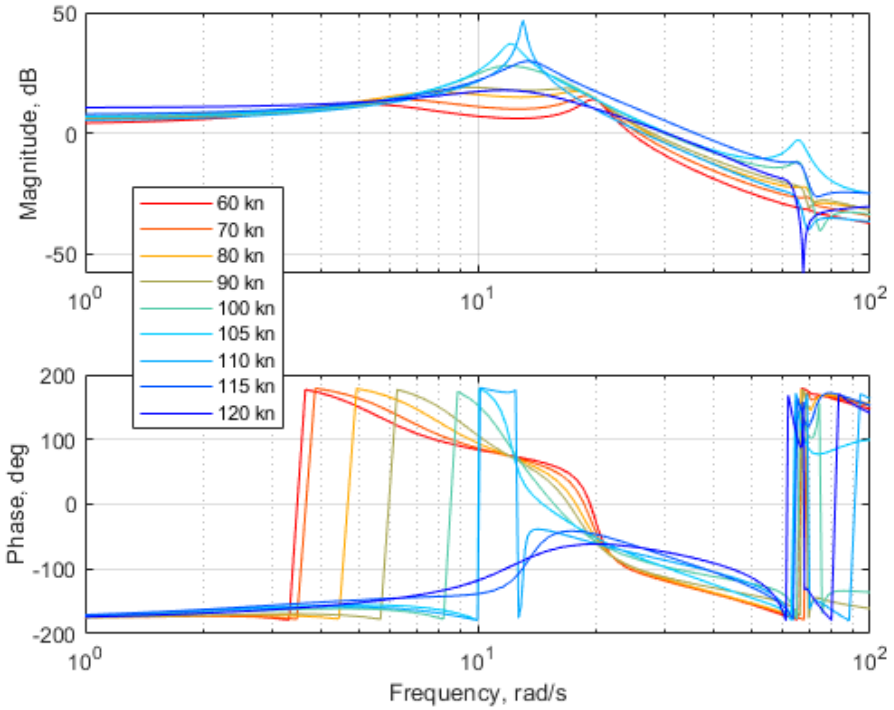

Figure 4-2: Low-order equivalent system frequency response overplot (wing flap 4 to pitch rate).

Figure 4-3 shows the results of the open-loop raps as the instability is approached. The left plot (110 kn and 30 lb of fuel) is marginally stable. As the aircraft burns off fuel the mode is destabilized. The center plot (110 kn and 23 lb of fuel) appears to be nearly neutrally stable, and the right plot (110 kn and 21 lb of fuel) shows that the mode is unstable with a slowly divergent pitch rate oscillation.

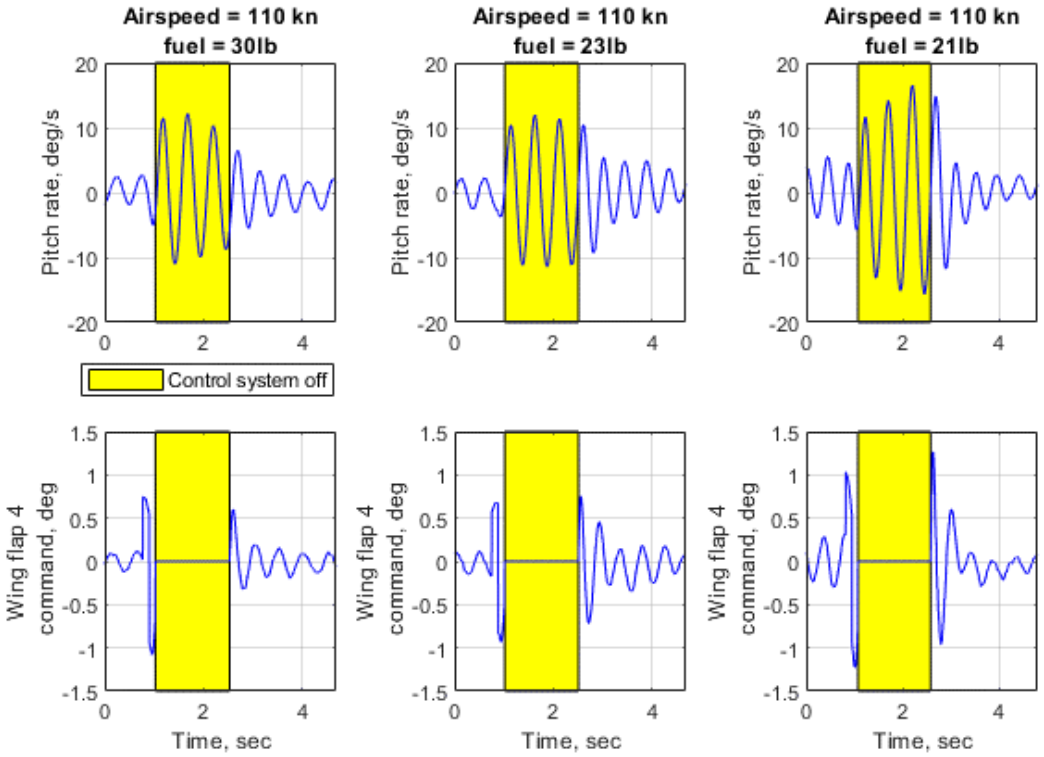

Figure 4-3: Open-loop rap: Stable (left); neutrally stable (center); and unstable (right).

5.0 CONCLUSIONS AND LESSONS LEARNED

Overall, the system and flight-test approach for the X-56A Multi-Utility Technology Testbed (Lockheed Martin, Bethesda, Maryland, U.S.A.) was highly successful and worked very well for testing up to and beyond flutter instabilities. The combined ground control station with pilot stations, control room, and simulation capabilities proved to be instrumental in facilitating the high level of team preparedness, coordination, communication, and situational awareness necessary for this kind of high-risk testing.

The flight-test maneuvers utilizing automatic flight-test aids were also a key enabler. Without these repeatable, highly specialized maneuvers, it would not have been possible to extract the necessary information from the flight-test data. Traditional flight-test maneuvers that utilize logarithmic frequency sweeps would not have been practical due to the long durations of the maneuvers needed to excite all of the frequencies of interest for the pertinent modes. The optimized multisine maneuvers yielded higher quality data in a fraction of the flight-test time required by traditional techniques.

The low-order equivalent system proved capable of capturing the complex flight dynamics to a very high degree. These systems were instrumental in extracting modal information, and provided key insights used for control system design leading up to the flutter instability. The modal information extracted by the low-order equivalent system combined with the Zimmerman flutter margin parameter yielded a very good estimate of the airspeed at which the flutter instability would occur, requiring very few flight-data points.

There are a number of significant lessons learned from the X-56A project that are applicable to designing and

operating medium- to high-risk unmanned aircraft of this class. Two lessons were learned the hard way because of project missteps, and some of them were understood from the beginning and facilitated the successful completion of the flight research objectives of the project.

The first lesson is to design the aircraft to be operationally robust. The X-56A aircraft were extremely difficult to operate due to challenges with takeoff and landing. The X-56A project team was originally so focused on the risks associated with flutter that the X-56A landing gear was designed primarily to survive a parachute landing in the event of an inflight wing failure. This design mindset resulted in landing gear that did not sufficiently absorb energy on landing and was the primary cause of the first incident. Those same landing gear design choices limited design flexibility relevant to takeoff rotation and were significant contributors to the second incident on takeoff. Neglecting seemingly mundane elements of the operation can lead to underestimating the risks associated with operating the aircraft. Takeoff and landing challenges greatly reduced the operational capacity of the X-56A aircraft, reducing the amount of research data that could be collected.

The second lesson is that when flying unmanned aircraft situational awareness is often a significant challenge. The X-56A ground control station was well laid out, with great consideration given to ensuring that the pilot and engineering displays were clean and presented all of the key information. Additionally, integrating the cockpit, simulation, and control room into a single asset allowed the team to train very effectively. Problems with the layout of the braking and throttle interfaces (combined onto a single inceptor), however, resulted in delays in decelerating the aircraft upon landing, which was a contributor to the first incident. Subsequent flights utilized a conventional throttle layout and rudder pedals with toe brakes in order to eliminate modal confusion and improve the human machine interface for landing. The X-56A project team utilized chase aircraft and external cameras very effectively to mitigate situational awareness deficits inherent to unmanned flight operations.

Finally, a project team must manage and communicate based on risk assessments. The first two incidents with the X-56A aircraft were treated as full National Aeronautics and Space Administration mishaps. While much was learned from the investigations, it was later realized that fundamentally the X-56A aircraft had been designed with the assumption that loss of the aircraft was an expected outcome. The X-56A aircraft was designed to be high-risk. A mishap exclusion memorandum was written to document the basic risk posture of the aircraft which simplified flight approvals and streamlined returning to flight after future anomalies. Taking too much operational risk can result in loss of the aircraft prior to achieving the goals of the project; however, being too risk-averse has the same outcome because resources are exhausted trying to drive risks below what is practical for the test mission. Risk posture should be a key driver at all stages of a project, from design to operations to mishap investigations. Unmanned aircraft test operations need to thread the needle between taking too much or too little risk, and constantly adapt.

FUNDING SOURCES

The X-56A Multi-Utility Technology Testbed (Lockheed Martin, Bethesda, Maryland, U.S.A.) was a collaboration between the National Aeronautics and Space Administration (NASA); the Air Force Research Laboratory (AFRL), and Lockheed Martin. Lockheed Martin built the aircraft under contract from the AFRL, and NASA took ownership of the aircraft at the end of that Lockheed/AFRL contract. NASA continued to operate the X 56A aircraft, and was partially funded by AFRL through the end of the of the project.

REFERENCES

[1] Beranek, J., Nicolai, L., Buonanno, M., Burnett, E., Atkinson, C., Holm-Hansen, B., and Flick, P.,

"Conceptual Design of a Multi-utility Aeroelastic Demonstrator," AIAA-2010-9350, 2010. DOI: 10.2514/6.2010-9350.

[2] Ryan, J., Bosworth, J., and Burken, J., and Suh, P., "Current and Future Research in Active Control of Lightweight, Flexible Structures Using the X-56 Aircraft," AIAA-2014-0597, 2014. DOI:10.2514/6.2014-0597.

[3] Baumann, E., *X-56A Buckeye Nose Gear Collapse*, 2015. All requests for public release should be forwarded to the Armstrong Flight Research Center Office of Chief Counsel. They can be reached at (661) 276-3997.

[4] Howe, S., *X-56 Crash Immediately After Takeoff Technical Mishap Investigation Report*, 2016. All requests for public release should be forwarded to the Armstrong Flight Research Center Office of Chief Counsel. They can be reached at (661) 276-3997.

[5] Ouellette, J., "Aeroservoelastic Modeling of Body Freedom Flutter for Control System Design," AIAA-2017-0019. DOI: 10.2514/6.2017-0019.

[6] Grauer, J., and Boucher, M., "Real-Time Estimation of Bare-Airframe Frequency Responses from Closed-Loop Data and Multisine Inputs," *Journal of Guidance, Control, and Dynamics*, Vol. 43, No. 2, February 2020, pp. 288-298. DOI:10.2514/1.G004574.

[7] Grauer, J., and Boucher, M., "Identification of Aeroelastic Models for the X-56A Longitudinal Dynamics Using Multisine Inputs and Output Error in the Frequency Domain," Aerospace 2019, 6, 24. DOI:10.3390/aerospace6020024.

[8] Morelli, E., *Identification of Low Order Equivalent System Models From Flight Test Data*, NASA TM-2000-210117, 2000.

[9] Mitchell, D., and Hoh, R., "Low-Order Approaches to High-Order Systems: Problems and Promises." *Journal of Guidance, Control, and Dynamics*, Vol. 5, No. 5, Sept.-Oct. 1982, pp. 482-489. DOI: 10.2514/3.56195.

[10] Pankonien, A., Suh, P., Schaefer, J., and Mitchell, R., "Deadbands Tell No Tails: X-56A Dynamic Actuation Requirements," SMASIS2020-2427, V001T03A016, 2020. DOI: 10.1115/SMASIS2020-2427.

[11] Zimmerman, N, and Weissenburger, J. "Prediction of Flutter Onset Speed Based on Flight Testing at Subcritical Speeds," *Journal of Aircraft*, Vol. 1, No. 4, July-August 1964, pp. 190-202. DOI: 10.2514/3.43581.